Green Chemistry

PAPER

Towards a scalable recycling process for ceramics in fuel-electrode-supported solid oxide cells†

Stephan Sarner, [a,b] Norbert H. Menzler, *[a,b] Jürgen Malzbender, [a]
Martin Hilger, [a,b] Doris Sebold, [a] André Weber [c] and Olivier Guillon [a,b,d]

The solid oxide cell (SOC) technology relies on high-performance ceramics containing strategically valuable and critical raw materials. This study focuses on the processing of spent cell materials from fuel-electrode-supported SOCs, demonstrating the feasibility of utilizing a significant portion of the ceramic cell in a closed-loop system. More than 85% of the cell's initial mass was directly incorporated into substrate manufacturing. The air-side perovskites were initially separated using hydrochloric acid treatment, followed by mechanical reprocessing of the remaining half cells. The performance of the resulting full cells containing 50 mass% recycled material in the substrate was evaluated, achieving a current density of up to 1.14 A cm^{-2} at 0.7 V and 750 °C in fuel cell mode, which is comparable to that of non-recycled counterparts. Preliminary experiments for the recovery of leached metal ions from the air electrode were conducted using direct oxalate precipitation while examining pH dependence. Direct oxalate precipitation proved particularly effective in the low pH range for the recovery of a lanthanum oxalate precursor with a purity exceeding 98%. The results highlight the potential for simple and sustainable practices in SOC technology.

Green foundation

1. This study demonstrates the successful reintegration of up to 50 wt% recycled material into SOC substrates without compromising cell performance. By enabling the direct reuse of critical raw materials like NiO, YSZ, and GDC, the work reduces the need for virgin resources and minimizes waste. The approach emphasizes scalable, selective material recovery, paving the way for more sustainable recycling solutions in ceramic technologies.

2. We successfully recycled over 85% of the total SOC mass in a closed-loop system. For the remaining 15%, an open-loop recovery method achieved lanthanum oxalate recovery with a purity of 98.3%. The use of recycled materials maintained substrate suitability and did not compromise cell performance, as evidenced by achieving a current density of 1.14 A cm^{-2} at 0.7 V in fuel cell mode, comparable to non-recycled cells. This demonstrates the viability of integrating recycled materials into manufacturing processes.

3. Future research could explore a hybrid leaching approach of mineral with organic acids to minimize environmental impact. Furthermore, a comprehensive life cycle assessment (LCA) could evaluate the environmental benefits of scaling the process.

1. Introduction

Hydrogen is widely recognized as a fundamental chemical element with profound implications for the global economy. It is also increasingly seen as a viable solution for energy conversion and storage, addressing the inherent intermittency of renewable energy sources, notably wind and solar power. In the field of established fuel cell and hydrogen technologies, solid oxide cells (SOCs) are emerging as a significant technology, distinguished by a number of key advantages compared to their competitors. These include their capacity to operate at

[a]*Institute of Energy Materials and Devices (IMD), Wilhelm-Johnen-Str., D-52425 Jülich, Germany. E-mail: n.h.menzler@fz-juelich.de*
[b]*Institute of Mineral Engineering (GHI), RWTH Aachen University., Forckenbeckstr. 33, D-52074 Aachen, Germany*
[c]*Institut für Angewandte Materialien – Elektrochemische Technologien (IAM-ET), Adenauerring 20b, D-76131 Karlsruhe, Germany*
[d]*JARA: Jülich-Aachen-Research-Alliance, D-52428 Jülich, Germany*
†Electronic supplementary information (ESI) available. See DOI: https://doi.org/10.1039/d4gc05883f

elevated temperatures, thus enabling the efficient co-generation of electricity and heat, their remarkable fuel versatility, and their proficiency in the efficient conversion of carbon-containing fuels into hydrogen or syngas. SOCs are therefore expected to play a pivotal role in driving the advancement of the hydrogen-based economy and demonstrated, as demonstrated by various operating systems of companies worldwide.[1,2] However, while research and development efforts have significantly improved the efficiency, reliability, and durability of SOCs, challenges related to long-term performance and the reduction of costs persist.[3,4] Ensuring cost competitiveness with other energy transition technologies remains a critical hurdle for its broad commercialization.

The manufacturing of established SOCs requires high-quality materials such as special metals and tailored ceramics, which are not only expensive but also limited in supply. While the ceramic core unit represents a minor fraction of the overall weight of the system, it still contains the most valuable raw materials. These include several rare earth elements such as lanthanum (La), yttrium (Y), cerium (Ce), gadolinium (Gd), strontium (Sr), cobalt (Co), and substantial quantities of the catalyst material nickel (Ni).[5] Each of these elements is classified as critical due to their occurrence and/or supply status, as per the EU's 2023 list of critical raw materials.[6] Moreover, the extraction and production of the required raw materials often generate significant carbon dioxide emissions, which have an adverse impact on the environment.[7] Through the comprehensive closure of material loops, the technology can significantly reduce its ecological footprint. Even contentious ethical aspects, such as working conditions in industrial cobalt mining[8] are addressed and can be mitigated through the reuse of components.

Ceramic cell recycling relies on the separation of the fundamental material units within the SOC system. These include the balance-of-plant (BoP) components, metallic interconnects, frames and end plates, contact materials, and finally, the ceramic cell components themselves. The disassembly of levelled stack components was suggested by Wright & Rahimifard (2012) as an initial step following the system shutdown.[9] More recently, Al Assadi et al. (2023) provided additional details on suitable disassembly techniques and associated challenges.[10] According to Wright & Rahimifard[9] and other related studies,[11–13] most of the separated components can be integrated into conventional, existing waste streams, with the aim of maintaining the value of the product. Nonetheless, there is still no standardization in place for materials, components, stack design, or disassembly strategies.

When it comes to the ceramics within SOCs in particular, reusability and recycling are an emerging area of research with no well-established recovery methods currently in place. Within the framework of the EU HyTechCycling project (2016–2019), Férriz et al. (2019) provided initial thoughts on the recycling of various fuel cell and hydrogen technologies, including SOCs.[13] Beyond covering the legislative aspects involved and the management of hazardous materials, the

authors proposed a potential recycling chain for all major system components. In contrast to the BoP components and the metallic components, it is unlikely that ceramic cells can be separated without damage and restored for reintegration into operational use. This is primarily attributed to the brittle nature of the ceramic cells and the stack sealant. In addition to potential cell breakage during disassembly, the cells degrade during operation. Multiple factors such as the duration of operation, the operating mode (electrolysis or fuel cell) and temperature, the gas composition and purity, internal stresses, and material selection influence the type and extent of degradation. End-of-use or end-of-life (EoU/EoL) cells may therefore exhibit a range of defects in comparison to their pristine counterparts. Notable reported defects include cell poisoning, layer delamination, cracking, oxidation, and interdiffusion.[14–17] The recycling process must therefore demonstrate a certain tolerance to potential variations in the condition of the input materials.

Until now, only a few studies have provided approaches for suitable recovery methods for the SOC ceramics. Valente et al. (2019)[18] suggested the recovery of yttria-stabilized zirconia (YSZ) through hydrothermal treatment, which was initially developed by Kamiya et al. in 2007.[19] The concept of hydrothermal-based recovery was then combined with an additional nickel leaching step with concentrated HNO_3, as explored in a study by Saffirio et al. (2022).[20] A comparable approach was undertaken by Yenesew et al. (2023), utilizing the recovered YSZ powder fraction for the production of new electrolyte material.[21] In both studies, fuel-electrode-supported cells (FESCs) were examined, and the air-side perovskite layer was manually removed by scraping/polishing before the actual recovery process commenced. An alternative mechanical removal of the air-side perovskites was successfully demonstrated by Kaiser et al. (2023).[22] In addition to the recycling of YSZ and nickel, Benedetto Mas et al. (2022) made suggestions for the recovery of lanthanum and cobalt, which is commonly present in the perovskite fraction of the SOC.[23] These suggestions rely on recovery processes applied for e-waste, battery, and spent catalyst materials.

For the successful recycling of SOC ceramics, the process must be cost-effective and designed for large-scale application. A closed-loop system thus enables the reuse of the EoU/EoL product for the same purpose, preserving its value. The previously applied concepts aim to separate not only the perovskite air electrode but also the nickel, and possibly even the gadolinium-doped cerium oxide (GDC) derived from the air-side diffusion barrier layer as single fractions. In the terms of reusing YSZ as an electrolyte material, precise separation is necessary, as both, ionic conductivity and electron insulation are significantly impaired by the presence of impurities. Although the recovery to YSZ electrolyte material may appear to be upcycling, it involves more processing/recovery steps and has a lower tolerance to impurities.

The process conducted in this work is an alternative possibility, which follows the concept presented in our own studies[12,24] and illustrated in Fig. 1. To follow this strategy, the
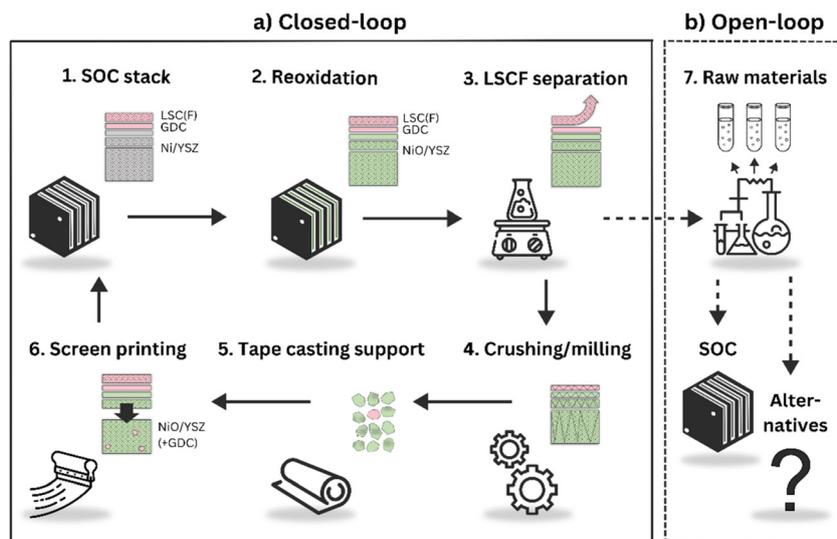
Fig. 1 Applied recycling concept for fuel-electrode-supported SOCs; (a) closed loop part and (b) open loop part of the concept.

ceramics are reprocessed into substrate material instead of electrolyte powder, favoring several important aspects: the substrate and fuel electrode of FESCs already consist of a YSZ and nickel cermet network, accounting for approximately 80% of the total cell weight.[12] The need for nickel separation is thus eliminated, simplifying the process and enabling the direct reuse of the majority of the recycled materials. Secondly, the substrate mainly serves for mechanical support, gas distribution, and electronic conduction. The presence of impurities may therefore assume a subordinate role when located in the substrate. In comparison to the electrodes and the electrolyte, the microstructure of the substrate is coarse and porous. Accordingly, the recycled powder does not require processing into the nanometer range, eliminating the need for disaggregation *via* hydrothermal treatment and high-power grinding steps. Finally, the challenge of achieving a scalable detachment of the air electrode and the GDC diffusion barrier from the remaining ceramic is addressed. Raw materials derived from the air electrode are extracted through leaching, while the GDC becomes an integral part of the substrate.

To summarize the concept outlined in Fig. 1, it can be broken down into two primary segments: the closed loop and the open loop. In the closed-loop segment, most of the ceramic becomes reprocessed into a new sintered substrate. Before system shutdown, the stack is flushed with air to ensure a complete oxidation of the nickel phase. This step is crucial, as nickel oxide serves as a raw material in cell manufacturing and exhibits enhanced stability when exposed to acidic leaching agents. The air electrode is subsequently separated through ultrasonic-assisted leaching. The remaining solids are processed into a powder, which is then integrated into the manufacturing of the substrate. In the open-loop segment, the components of the air electrode are restored from the solution and can be employed for SOC or alternative applications.

This study introduces several novel aspects, including an evaluation of various diluted acids for the partial dissolution of the air electrode from the full cell assembly, a detailed investigation of the recycled powder/sintered ceramic after each processing step, and the validation of the recycling approach through single cell testing. Furthermore, a potential recovery pathway for the dissolved air electrode *via* oxalic acid precipitation is proposed.

2. Results and discussion

2.1. Closed-loop recovery

The closed-loop recycling process (Fig. 1a) is divided into the chemical separation of the perovskite (section 2.1.1) and the mechanical reprocessing steps for its incorporation into the new substrate material, which is then validated by single-cell testing (section 2.1.2).

2.1.1 Leaching of cell components. The air-side separation involves comparing the leaching efficiency of LSCF using eight different types of acids. The objective is to maximize the leaching of LSCF, while ensuring the stability of YSZ, NiO, and – preferably – GDC.

Under the investigated conditions, the YSZ fraction exhibits the highest stability. The highest leaching efficiency for YSZ is $1.49 \pm 0.02\%$, which is observed under the most severe leaching conditions with HCl (80 °C, 4 h contact time, with the addition of 3 vol% H_2O_2). The GDC fraction demonstrates stability under moderate leaching conditions. However, it also exhibits a tendency to dissolve, particularly at elevated temperatures. The highest leaching efficiency for GDC was found to be $48.52 \pm 4.02\%$ using H_2SO_4 under the most severe leaching conditions (80 °C, 4 h contact time, with the addition of 3 vol% H_2O_2). Similar to GDC, the leaching of NiO is significantly affected by temperature. The most promising results
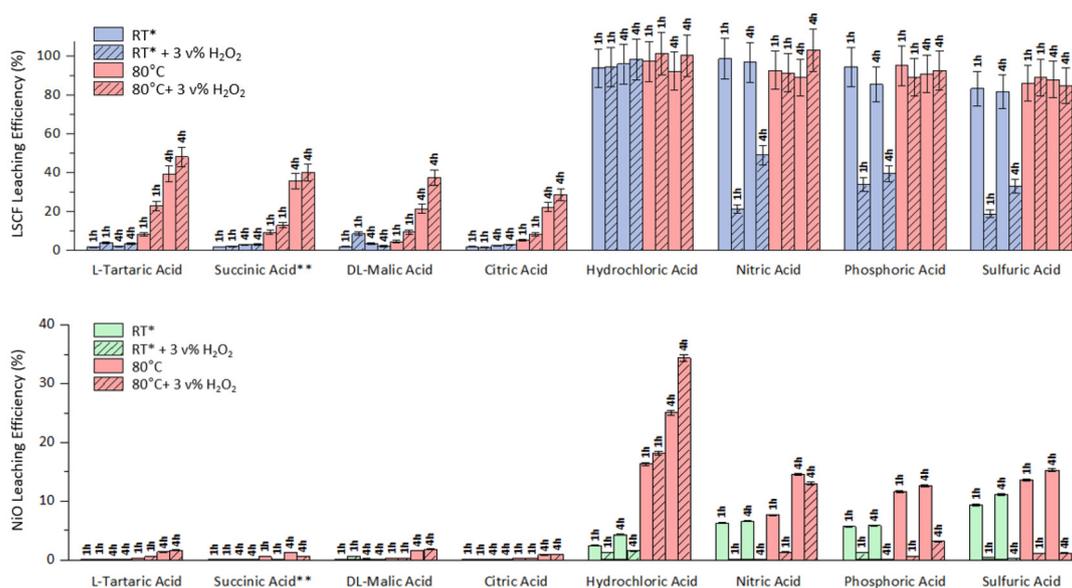
Fig. 2 Leaching efficiency of LSCF and NiO evaluated on ground full cell powder. Organic acid concentration is 2 M (exception: **succinic acid = 0.5 M), and mineral acid concentration is 6 M. Solid-to-liquid ratio is kept constant at 1 : 60. Error bars represent the relative standard deviation of the powder's heterogeneity. *RT room temperature.

were obtained by the mineral acids HCl and HNO_3 at room temperature (Fig. 2). Within the range of the relative error, LSCF leaching achieves up to 100% efficiency, while NiO leaching can be minimized to 0.10–6.53 ± 0.1% at the same time. Additionally, both YSZ and GDC leaching is mitigated significantly. When using HCl at room temperature, maximum leaching of YSZ can be expected with 0.54 ± 0.01%, and for GDC, 4.62 ± 0.38%. When using HNO_3 at room temperature, maximum YSZ leaching is 0.07 ± 0.01%, and GDC leaching is 15.81 ± 1.31%. On the other hand, none of the organic acids utilized are able to dissolve LSCF sufficiently. The most favorable results were achieved with tartaric acid under the harshest leaching conditions (80 °C, 4 h contact time, with the addition of 3 vol% H_2O_2), reaching a maximum leaching efficiency of 48.1 ± 5.1%.

For the recycling of the full cell parts, 6 M HCl was utilized at room temperature to separate the air electrode, while all other ceramic components, including NiO should remain stable. After 2 h contact time, the leaching process was halted. Table 1 presents the cell composition of cell batches 1 and 2 before and after the leaching process. Following the leaching, LSCF traces could not be detected by ICP-OES analysis in the remaining solid. The final composition of both cell batches is very similar, with only a slight difference in the GDC content, ranging from 1.4 mass% (cell batch 2) to 1.9 mass% (cell batch 1).

2.1.2 Reprocessing of ceramics into recycled substrate/cells. The sintered bodies that remained stable during leaching underwent the closed-loop recovery process, including the grinding, tape casting of the support, and ultimately, the full cell manufacturing (Fig. 1a, step 4–6). For cell batch 1, the solid fraction amounts to 84.5 mass% and for cell batch 2 it

amounts to 89.3 mass% in relation to the total cell weight before leaching. The starting powder and resulting substrate properties from the closed-loop process are listed in Table 2.

In each case, the recycled powder/slurry/substrate is compared to the pristine counterpart, which does not contain any recyclate.

When examining the chemical composition of the pristine raw powder and the recycled cell powder, two major differences emerge. Firstly, small quantities of the GDC barrier are present, and secondly, the ratio of NiO to YSZ is slightly smaller in the recycled powder. The reason for the disturbed NiO to YSZ ratio can be attributed to the presence of the electrolyte in the recycled powder, which consists solely of YSZ. Despite adjusted leaching conditions, small amounts of nickel oxide dissolve into the solution, while YSZ remains highly stable.

The cell fragments were subjected to grinding to align the particle size and the specific surface area with that of the pristine raw powder. The particle size distribution is indicated by the D10, D50, and D90 values. The D50 value is 1.44 μm for the pristine raw powder and 1.43 μm (batch 1) or 1.46 μm (batch 2) for the recycled material, respectively. The specific surface area is within the same order of magnitude, with the recycled cell material showing slightly higher values, indicating minor differences in grain morphology. The viscosity data of the standard and partially recycled slurry at an equivalent shear rate of 10 s^{-1} are very similar. The flow and drying behavior of the slurry during the tape casting process were therefore found to be similar, with no instances of drying defects detected.

However, after the sintering of the green tapes, notable differences emerge in the shrinkage behavior and the resulting

Table 1 Normalized chemical composition of full cells before and after leaching in 6 M HCl. Errors provided as relative standard deviation

Cell fraction	Oxide	Before leaching (mass%)		After leaching (mass%)	
		Cell batch 1	Cell batch 2	Cell batch 1	Cell batch 2
Substrate, fuel electrode, electrolyte (NiO/YSZ)	ZrO_2	33.24 ± 0.25	33.83 ± 1.30	37.51 ± 0.80	37.55 ± 0.95
	Y_2O_3	3.35 ± 0.02	3.28 ± 0.08	3.65 ± 0.07	3.86 ± 0.12
	NiO	46.90 ± 0.25	51.29 ± 1.87	56.96 ± 1.02	57.26 ± 1.21
Barrier layer (GDC20)	CeO_2	1.49 ± 0.02	0.65 ± 0.04	1.47 ± 0.02	0.97 ± 0.08
	Gd_2O_3	0.50 ± 0.01	0.26 ± 0.02	0.41 ± 0.01	0.36 ± 0.02
Air electrode (LSCF)	La_2O_3	2.03 ± 0.02	4.80 ± 0.37	bdl[a]	bdl[a]
	SrO	1.20 ± 0.01	2.06 ± 0.15	bdl[a]	bdl[a]
	CoO	0.32 ± 0.01	0.72 ± 0.05	bdl[a]	bdl[a]
	FeO	1.73 ± 0.01	3.11 ± 0.24	bdl[a]	bdl[a]
Contact layer (LCC10)	La_2O_3	6.35 ± 0.02	—	bdl[a]	—
	MnO_2	1.33 ± 0.03	—	bdl[a]	—
	CoO	1.00 ± 0.01	—	bdl[a]	—
	CuO	0.57 ± 0.01	—	bdl[a]	—
Sum		100	100	100	100

[a] bdl below detection limit.

Table 2 Results on the sample properties during different states within the recycling process of two cell batches. Errors provided as standard deviation

Sample state	Property	Unit	Cell batch 1			Cell batch 2		
			0% recyclate	25% recyclate	50% recyclate	0% recyclate	25% recyclate	50% recyclate
Powder	YSZ share	mass%	40.0	41.2	41.2	40.0	41.4	41.4
	NiO share	mass%	60.0	57.0	57.0	60.0	57.3	57.3
	GDC share	mass%	0.0	1.9	1.9	0.0	1.3	1.3
	LSCF share	mass%	0.0	bdl[a]	bdl[a]	0.0	bdl[a]	bdl[a]
	Particle size D10	μm	0.56	0.48	0.48	0.56	0.42	0.42
	Particle size D50	μm	1.44	1.43	1.43	1.44	1.46	1.46
	Particle size D90	μm	3.58	3.71	3.71	3.58	3.99	3.99
	Specific surface area	$m^2\ g^{-1}$	2.47	3.26	3.26	2.47	2.77	2.77
Slurry	Viscosity at shear rate $10\ s^{-1}$	Pa s	6.1	8.4	10.8	6.6	8.6	10.8
Substrate	In-plane shrinkage, lateral	%	17.39 ± 1.14	16.00 ± 0.40	15.11 ± 0.68	16.81 ± 0.77	15.06 ± 2.63	15.38 ± 2.55
	In-plane shrinkage, vertical	%	17.60 ± 0.37	16.52 ± 0.15	15.58 ± 0.13	17.48 ± 0.34	16.61 ± 1.37	15.37 ± 1.38
	Porosity (oxidized)	vol%	6.32 ± 0.79	9.06 ± 0.70	11.90 ± 1.58	6.66 ± 0.42	10.69 ± 3.5	16.23 ± 2.13
	Porosity (reduced)	vol%	24.74 ± 3.53	29.56 ± 1.99	31.85 ± 1.51	26.73 ± 1.44	32.85 ± 0.84	35.37 ± 1.04
	Substrate thickness (oxidized)	μm	493 ± 35	509 ± 5	529 ± 7	532 ± 45	514 ± 6	533 ± 13
	Substrate thickness (reduced)	μm	540 ± 22	503 ± 9	517 ± 4	588 ± 6	527 ± 24	514 ± 11
	NiO:YSZ ratio (oxidized)	N	1.40 ± 0.03	1.37 ± 0.02	1.31 ± 0.07	1.42 ± 0.03	1.38 ± 0.04	1.38 ± 0.04

[a] bdl below detection limit.

porosity of the substrates. Incorporating recycled material into the standard slurry is expected to reduce sintering shrinkage, thus leading to an increase in porosity (Fig. 3). The relationship between the decrease in the in-plane shrinkage (eqn (1)) and the increase in porosity (eqn (2)) can be expressed using linear regression as follows:

$$\text{Shrinkage decrease } s(r) = -mr + c \quad (1)$$

$$\text{Porosity increase } p(r) = mr + c \quad (2)$$

where: m is the slope of the regression line, representing the rate of change in shrinkage/porosity with respect to the re-

cycling amount. r is the relative amount of pristine powder replaced with the recycled powder. c is the y-intercept of the regression line, representing the baseline shrinkage/porosity when no recycled material is added.

In both the powder and substrate sample states, the recycled material exhibits similar particle shapes and sizes compared to the pristine material. The microstructure of the recycled cermet is defect-free, the disparity in porosity is clearly evident. Sintering activity might be influenced due to the initial processing of the ceramic particles, resulting in less shrinkage during the second sintering (recycling process). To address this issue, three potential approaches might be considered. Firstly, adjust-
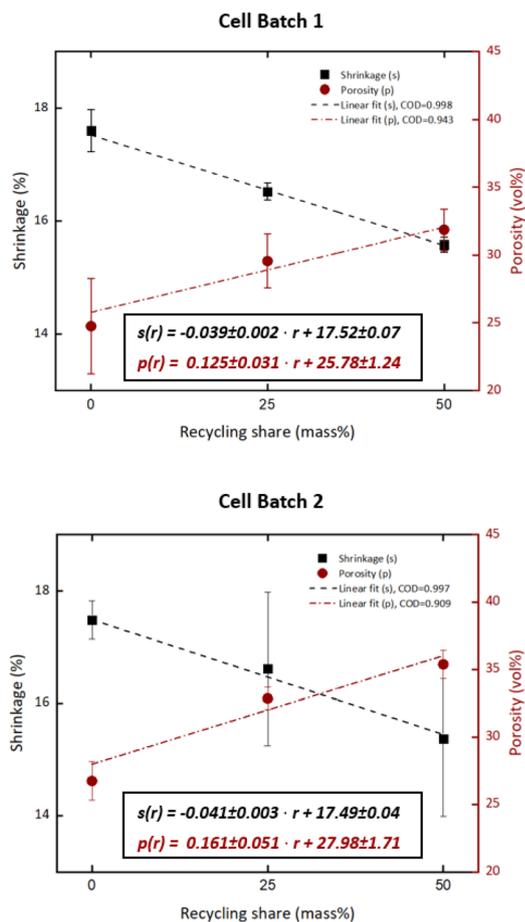
Cell Batch 1

$s(r) = -0.039\pm0.002 \cdot r + 17.52\pm0.07$

$p(r) = 0.125\pm0.031 \cdot r + 25.78\pm1.24$

Cell Batch 2

$s(r) = -0.041\pm0.003 \cdot r + 17.49\pm0.04$

$p(r) = 0.161\pm0.051 \cdot r + 27.98\pm1.71$

Fig. 3 Sintering shrinkage (in-plane, vertical) and porosity of partially recycled and non-recycled fuel-electrode-supported substrates and corresponding linear fits with coefficient of determination (COD). Error bars given as standard deviation.
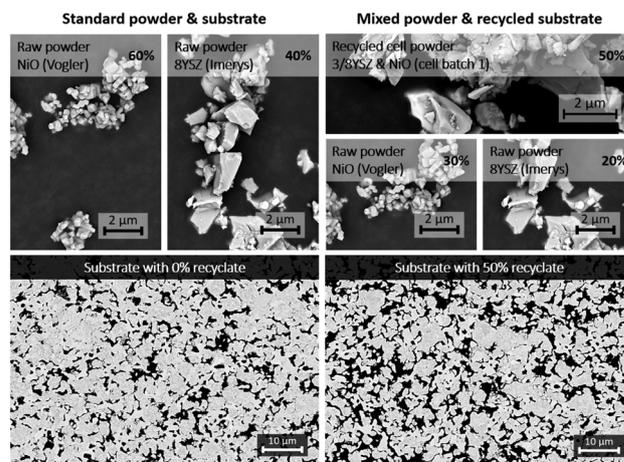

Fig. 4 Backscattered electron images of raw powders used for substrate processing and resulting microstructure of substrates with 0% and 50 mass% recyclate by weight (cell batch 1). Both substrates shown are sintered at 1400 °C and subsequently reduced at 900 °C in H_2/Ar.

ing particle size to achieve a narrower/smaller distribution might enhance surface area and sinterability. Secondly, subjecting the sintered bodies to an additional hydrothermal treatment after grinding might help to separate NiO from YSZ particles, thus further increasing the surface area.[19] Finally, modifying the sintering program to longer pre-sintering holding times or slightly higher end-sintering temperatures may be beneficial. However, such adjustments could potentially introduce drawbacks to the microstructure evolution of the subsequent functional layers to be applied. Conversely, an increase in substrate porosity might enhance the transport of reactant gases to the active cell area. If mechanical stability and electrical conductance are adequately maintained, higher porosity could even prove beneficial.

The resulting porosity changes in the substrates are shown in two backscattered electron images (Fig. 4), comparing the pristine to the recycled substrates.

A rise in porosity typically results in reduced mechanical stability, lower fracture toughness, and fracture strength due to the initiation of cracks from pores in ceramic networks,[25,26] which is also verified in studies on SOC materials.[27] This corre-lation was indeed also observed for the current experimental results on the fracture strength. Table 3 presents the mechanical properties of oxidized and reduced substrates with different recycling amounts. In general, oxidized samples demonstrate higher fracture strengths and Young's modulus compared to reduced ones. This is also observed for comparable material compositions and substrate thicknesses,[28] while fracture strain increases in the reduced state. Oxidized samples thus tend to sustain higher stresses before fracture but exhibit less elastic behavior. In the reduced sample state, increasing the recycling amount tends to lead to decreased mechanical stability, although the scattered data only provide indications.

Fig. 5 depicts the fracture strength data based on the recycling amount within the substrates. The averaged fracture strengths for samples at elevated temperatures are distributed within the dataset of the corresponding room temperature samples. The absolute values for the calculated fracture strengths are reasonable compared to similar material compositions and substrate thicknesses investigated in the literature.[28,29]

2.1.3 Full cell testing. After reduction, all cells showed a sufficient gas tightness. The open-circuit voltage (OCV) at 800 °C in synthetic air/dry H_2 revealed minor leakages of 0.72% to 1.18% steam in the fuel gas. Accordingly, the differences in the OCV of the four cells were below 4 mV in the subsequent tests.

In the initial 24 h stability test, none of the cells showed any degradation, proving that there is no severe poisoning effect introduced by impurities in the recyclate. Similar results were found in a study by Saffirio *et al.* (2024),[30] where half-cell scrap was partially incorporated into substrate material. The single-cell performance results from this study (SOFC and SOEC mode) are summarized in Fig. 6a. The upper lines show the SOFC current density achieved at a cell voltage of 0.7 V

Table 3 Mechanical properties of reduced and oxidized substrates (cell batch 1) fractured at room temperature and at 800 °C. Errors given as standard deviation, errors for Weibull modulus given in a 95% confidence interval

Temperature	Mechanical property	Unit	0% recyclate	25% recyclate	50% recyclate
RT[a] (oxidized)	Fracture strength	MPa	154 ± 31	154 ± 22	146 ± 26
	Weibull's modulus	—	$4.8^{6.1}_{3.3}$	$7.7^{9.7}_{5.3}$	$6.2^{7.8}_{4.3}$
	Young's modulus	GPa	80 ± 19	95 ± 20	93 ± 18
	Fracture strain	%	0.19 ± 0.02	0.17 ± 0.03	0.16 ± 0.02
RT[a] (reduced)	Fracture strength	MPa	113 ± 21	100 ± 18	88 ± 18
	Weibull's modulus	—	$5.5^{7.0}_{3.8}$	$6.2^{7.8}_{4.3}$	$5.0^{6.3}_{3.5}$
	Young's modulus	GPa	45 ± 9	37 ± 8	29 ± 6
	Fracture strain	%	0.26 ± 0.04	0.28 ± 0.04	0.30 ± 0.03
800 °C (oxidized)	Fracture strength	MPa	182 ± 24	185 ± 31	119 ± 42
	E-modulus	GPa	85 ± 23	95 ± 14	75 ± 18
	Fracture strain	%	0.22 ± 0.05	0.20 ± 0.04	0.16 ± 0.03
800 °C (reduced)	Fracture strength	MPa	103 ± 6	97 ± 9	79 ± 25
	E-modulus	GPa	17 ± 3	19 ± 4	12 ± 5
	Fracture strain	%	0.64 ± 0.11	0.52 ± 0.07	0.67 ± 0.07

[a] RT room temperature.
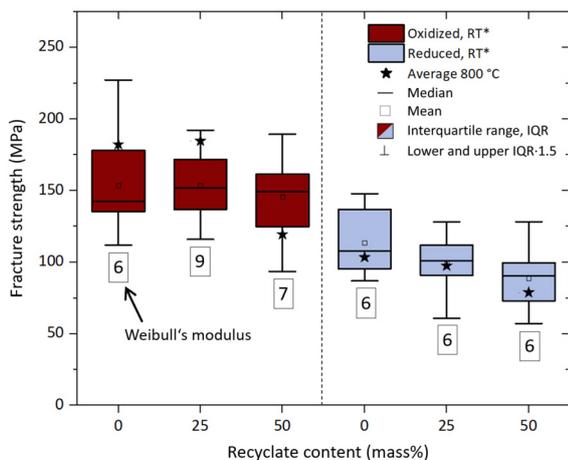
Fig. 5 Boxplots of the calculated fracture strength data and corresponding Weibull's modulus for room temperature (*RT) samples and average fracture strength of substrates at 800 °C.

(positive current) and the lower array of curves show the SOEC current densities at 1.2 V. While the two cells with 50% recyclate show similar performance values, the standard cells reveal different performances that are both lower than the performance of the cells with 50% recyclate. Fig. 6b and c reveal the impedance spectra and related distributions of relaxation times of the four cells measured at 750 °C in air/50%H_2 + 50% H_2O at OCV conditions. All cells show quite similar series resistances of 97–115 mΩ cm^2, proving that a sufficient contacting of the 1 cm^2 active electrode areas was achieved and that there is no severe impact of the recyclate on the electrolyte conductivity. However, significant differences in the polarisation resistance can be observed. Once again, the two cells with 50% recyclate show excellent agreement, whereas standard cell B shows a much higher polarization resistance. The distribution of relaxation times (DRT) is presented in Fig. 6c.
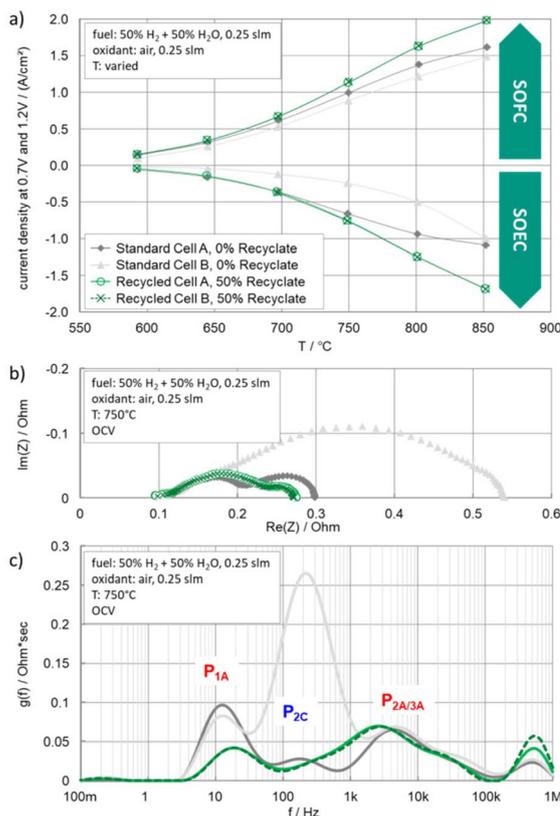
Fig. 6 Comparison of standard and recycled single-cell performance at 0.7 V and in the temperature range of 650–850 °C. (a) Current density versus temperature in fuel cell and electroylsis cell mode. (b) Impedance spectroscopy (EIS) in Nyquist plot. (c) From Fig. 6b derived distribution of relaxation times (DRT).

The results are consistent with previous studies[31,32] and reveal that the increase in polarization resistance is related to a dominant peak at ~200 Hz. This peak P_{2C} was clearly linked to the

LSCF air electrode in previous studies performed on the Jülich FESCs and other FESCs.[33,34] The insufficient performance of the air electrode is likely a consequence of the green tapes being shaped using a cutting plotter. As a result, not all of the cells achieved a sufficient flatness, which seemed to have an effect on the application of the LSCF air electrode layer. The performance of this cell should therefore not be considered further. With respect to P_{1A} in the DRT, a peak that is attributed to the gas diffusion in the substrate, the results are in agreement with the determined porosities of the two different substrates. While the standard cells exhibited a porosity of just 27%, the addition of the recyclate increased the porosity to 35%. Such an increase in porosity typically decreases the tortuosity, which was not determined in the microstructural analysis of these cells. As the gas diffusion polarization resistance is proportional to the tortuosity/porosity ratio,[33] the significant decrease in the P_{1A} peak is to be expected.

The charge transfer and coupled ionic and gas phase transport in the functional layer of the fuel electrode,[35] represented by P_{2A} and P_{3A} in the DRT, is only affected to a minor extent. The increased values of $g(f)$ in the range from 300 Hz to 1 kHz are at least partly related to the regularization in the DRT calculation. There seems to be at least no significant impact of the recyclate in the substrate on the performance of the fuel electrode functional layer. It should be noted again that this layer was made from standard materials without any recyclate.

2.2 Open-loop recovery

The open-loop recovery (Fig. 1b) is concerned with the mixed perovskite solution, referring to 14.5% of the entire EoU-cell mass (cell batch 1). To consider the recovery of La from the acidic solution, which represents the most substantial fraction both in terms of mass and cost, oxalate precipitation emerges as a favorable method. Oxalates of the rare earth elements (REE) are highly insoluble in acidic solutions, enabling the separation of pure products.[36–38] However, extracting other single-phase oxalates from solutions that contain various metal species is challenging. The precipitation of oxalates, whether individually or in combination, depends on factors such as pH as well as the presence, quantity, and valence state of the metal ion species in the solution. Transition metals like Fe, Co, or Ni tend to form more soluble complexes, which is contingent upon their valence.[39–41] Through the reoxidation step within the recycling process (Fig. 1a, step 2), the metal ions are initially in an oxidized state. However, they can undergo changes in their valence due to the mild reducing properties of the oxalic acid, influencing the precipitation point and efficiency. In order to establish a starting point for future recovery procedures of single or multiple raw materials from (acidic) perovskite solutions, the pH dependence of oxalic acid precipitation was examined at constant room temperature. Fig. 7 illustrates the XRD spectra of all precipitates at distinct pH values. The reflexes are normalized to the highest intensity observed within the diffractogram of each sample.

Given the challenges in distinguishing oxalate phase reflexes, only major reflexes were qualitatively identified and compared with existing literature data.[41–48] Additionally, Fig. 7 presents ICP-OES data of the solution composition, both before the initiation of the process and after its completion, reaching pH 10.

In the low pH range of 0–1, the formation of REE oxalates is predominant. The recovered La oxalate hydrate at pH 0 exhibits a purity of 98.3%, with primary impurities comprising 0.6% Sr, 0.5% Ce, and 0.3% Gd. This fraction represents 51.0% of the total mass of all precipitates. Up to pH 2, La oxalate precipitation persists, accompanied by increasing
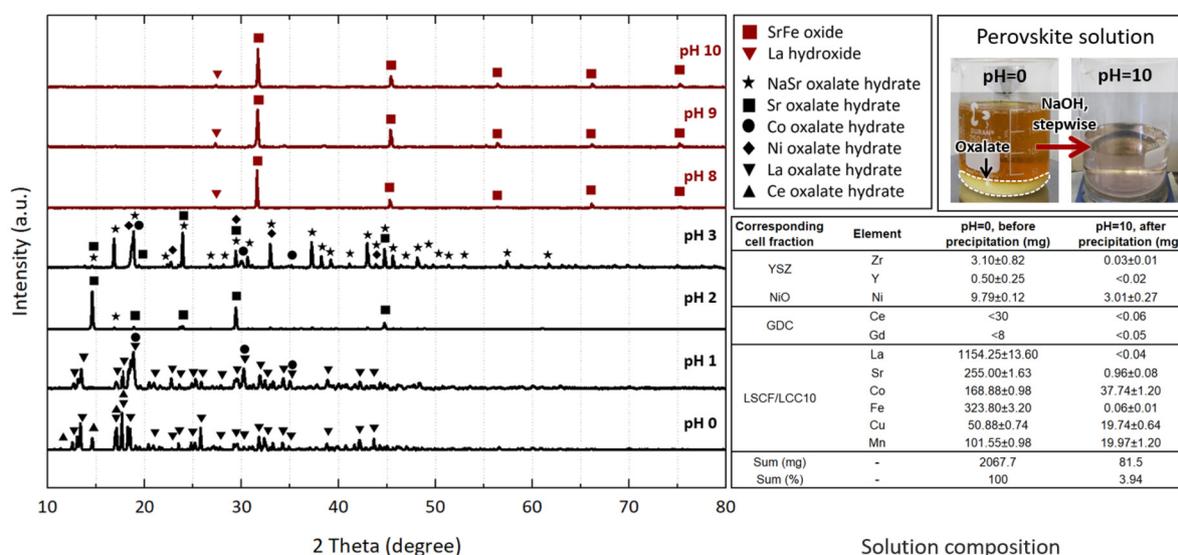

Corresponding cell fraction	Element	pH=0, before precipitation (mg)	pH=10, after precipitation (mg)
YSZ	Zr	3.10±0.82	0.03±0.01
	Y	0.50±0.25	<0.02
NiO	Ni	9.79±0.12	3.01±0.27
GDC	Ce	<30	<0.06
	Gd	<8	<0.05
LSCF/LCC10	La	1154.25±13.60	<0.04
	Sr	255.00±1.63	0.96±0.08
	Co	168.88±0.98	37.74±1.20
	Fe	323.80±3.20	0.06±0.01
	Cu	50.88±0.74	19.74±0.64
	Mn	101.55±0.98	19.97±1.20
Sum (mg)	-	2067.7	81.5
Sum (%)	-	100	3.94

Fig. 7 Normalized XRD spectra of oxalate phases recovered at different pH values (left) and macroscopic view of the perovskite solution before and after the pH increase, along with the corresponding total ion content of the solution, determined by ICP-OES (right). Sodium is omitted from the ICP-OES measurements, as it originates from the pH increasing agent.

impurities of Co, Cu, Mn, Ni, and Sr. Not all impurities detected by ICP-OES were clearly identified in the XRD diffractogram. At pH 2, Sr precipitation dominates, with impurities of Mn, La, and Na (pH-increasing agent) mostly detected *via* ICP-OES. From pH 2 to 3, the formation of mixed oxalates is observed, and Fe starts to precipitate. However, beyond this point, the solubility of remaining metal ions in the solution (mainly Fe, Mn, Cu, and Co) is sufficient to impede further precipitation. In a higher pH range of 8–10 residues of Fe, Sr, and Mn are recovered as hydroxides/oxides. The overall recovery efficiency is 96.1%, which is calculated by comparing the total ion content in the residual solution to that in the initial solution (Fig. 7).

The delayed precipitation of Fe indicates its presence mainly in the Fe(III) state. In contrast to the direct oxalate precipitation applied in this study, a neutralization route according to Venkatesan *et al.* (2018)[49] may be considered. In this case, the insolubility of REEs up to a pH value of approximately 7.5 is harnessed. Meanwhile, all trivalent and even some divalent impurities may be fully hydrolyzed and removed in a low pH regime before oxalate recovery commences.

To conclude, direct oxalate precipitation might be suitable to recover a relatively pure La oxalate phase, which can be used as a precursor material for perovskite manufacturing. Without any pre-treatment, the mixed oxalate phases recovered at intermediate to high pH regimes are unsuitable for SOC applications. Further optimization of the open-loop recovery process is needed, particularly in terms of pH regime, precipitation temperature, and oxalic acid consumption. Due to the advantageous molar surplus of oxalic acid in relation to precipitation yield, the recovery of oxalic acid following precipitation should be considered. The recycling of the perovskite-rich solution could therefore be linked to a suitable recovery process of oxalic acid, for example cooling crystallization, proposed by Liu *et al.* (2019).[50]

3. Conclusion

In this study, we conducted a recycling process for fuel-electrode-supported SOCs using waste material from two different cell batches. Over 85% of the total cell material was recycled in a closed-loop system, while for the remaining fraction (less than 15% by mass), an initial open-loop recovery approach was demonstrated.

Air-side separation is essential to initiate the recycling process. Various organic and inorganic acids were tested to dissolve LSCF while preserving the stability of YSZ, GDC, and NiO. The most promising results were obtained using 6 M HCl at room temperature, with a solid-to-liquid ratio of 1 : 5 and 2 hours of contact time. After leaching, the solid residues were reprocessed into a new substrate, with recycling rates of up to 50% by mass. Using recycled material instead of pristine raw powders affects sintering shrinkage to a certain extent, leading to increased substrate porosity. Both shrinkage decrease and porosity increase follow linear trends. In contrast to the oxi-

dized state, where strength remains rather constant, the mechanical strength of the reduced substrates appeared to slightly decrease with a higher recyclate content due to increasing porosity, although the substrates appear to remain suitable for full cell manufacturing. The results of the single-cell tests indicate that incorporating up to 50 mass% recycled material in the substrate does not compromise cell performance.

For the open-loop recovery, oxalate precipitation seems promising due to the high concentration of dissolved La in the leachate. We investigated the pH dependence of the system to provide a starting point for future perovskite recovery. At a low pH, the formation of La oxalate hydrate was predominant. About 51% of the total ion mass precipitated was recovered as an La oxalate single phase with a purity of 98.3%. Other oxalates/hydroxides were recovered as multi-phases, resulting in an overall recovery efficiency of 96.1%. However, these mixed phases may not be directly reusable for new perovskite synthesis.

Author contributions

Data availability

The authors confirm that the data supporting the findings of this study are available within the ESI.†

Conflicts of interest

There are no conflicts of interest to declare.

Acknowledgements

ance in conducting the leaching experiments and for their comprehensive execution of the ICP-OES analysis and data collection/evaluation.

References

1 M. C. Williams, S. D. Vora and G. Jesionowski, *ECS Trans.*, 2020, **96**, 1.

2 O. Corigliano, L. Pagnotta and P. Fragiacomo, *Sustainability*, 2022, **14**, 15276.

3 J. H. Prosser, B. D. James, B. M. Murphy, D. S. Wendt, M. J. Casteel, T. L. Westover and L. T. Knighton, *Int. J. Hydrogen Energy*, 2024, **49**, 207–227.

4 M. Lamagna, D. Groppi and B. Nastasi, *Int. J. Hydrogen Energy*, 2023, **48**, 27033–27058.

5 S. Harboe, A. Schreiber, N. Margaritis, L. Blum, O. Guillon and N. H. Menzler, *Int. J. Hydrogen Energy*, 2020, **45**, 8015–8030.

6 I. Directorate-General for Internal Market, M. Grohol and C. Veeh, *Study on the critical raw materials for the EU 2023: final report*, Publications Office of the European Union, LU, 2023.

7 M. Mori, R. Stropnik, M. Sekavčnik and A. Lotrič, *Sustainability*, 2021, **13**, 3565.

8 B. K. Sovacool, *Extr. Ind. Soc.*, 2019, **6**, 915–939.

9 E. I. Wright and S. Rahimifard, in *Leveraging Technology for a Sustainable World*, ed. D. A. Dornfeld and B. S. Linke, Springer, Berlin, Heidelberg, 2012, pp. 185–190.

10 A. Al Assadi, D. Goes, S. Baazouzi, M. Staudacher, P. Malczyk, W. Kraus, F. Nägele, M. F. Huber, J. Fleischer, U. Peuker and K. P. Birke, *Resour. Conserv. Recycl. Adv.*, 2023, **19**, 200172.

11 J. S. Cooper, S. Grot and C. Hartnig, in *Polymer Electrolyte Membrane and Direct Methanol Fuel Cell Technology*, ed. C. Hartnig and C. Roth, Woodhead Publishing, 2012, vol. 1, pp. 117–134.

12 S. Sarner, A. Schreiber, N. H. Menzler and O. Guillon, *Adv. Energy Mater.*, 2022, **12**, 2201805.

13 A. M. Férriz, A. Bernad, M. Mori and S. Fiorot, *Int. J. Hydrogen Energy*, 2019, **44**, 12872–12879.

14 A. Hauch, S. D. Ebbesen, S. H. Jensen and M. Mogensen, *J. Electrochem. Soc.*, 2008, **155**, B1184.

15 S. E. Wolf, F. E. Winterhalder, V. Vibhu, L. G. J. de Haart, O. Guillon, R.-A. Eichel and N. H. Menzler, *J. Mater. Chem. A*, 2023, **11**, 17977–18028.

16 S. J. McPhail, S. Frangini, J. Laurencin, E. Effori, A. Abaza, A. K. Padinjarethil, A. Hagen, A. Léon, A. Brisse, D. Vladikova, B. Burdin, F. R. Bianchi, B. Bosio, P. Piccardo, R. Spotorno, H. Uchida, P. Polverino, E. A. Adinolfi, F. Postiglione, J.-H. Lee, H. Moussaoui and J. Van herle, *Electrochem. Sci. Adv.*, 2022, **2**, e2100024.

17 T. L. Skafte, J. Hjelm, P. Blennow and C. R. Graves, in *Proceedings of 12th European SOFC & SOE Forum 2016*, European Fuel Cell Forum, 2016, pp. 8–27.

18 A. Valente, D. Iribarren and J. Dufour, *Int. J. Hydrogen Energy*, 2019, **44**, 20965–20977.

19 M. Kamiya, Y. Mori, T. Kojima, R. Sasai and H. Itoh, *J. Mater. Cycles Waste Manage.*, 2007, **9**, 27–33.

20 S. Saffirio, S. Pylypko, S. Fiorot, I. Schiavi, S. Fiore, M. Santarelli, D. Ferrero, F. Smeacetto and S. Fiorilli, *Sustainable Mater. Technol.*, 2022, **33**, e00473.

21 G. T. Yenesew, E. Quarez, A. Le Gal La Salle, C. Nicollet and O. Joubert, *Resour., Conserv. Recycl.*, 2023, **190**, 106809.

22 C. Kaiser, T. Buchwald and U. A. Peuker, *Green Chem.*, 2024, **26**, 960–967.

23 A. Benedetto Mas, S. Fiore, S. Fiorilli, F. Smeacetto, M. Santarelli and I. Schiavi, *Sustainability*, 2022, **14**, 3335.

24 S. Sarner, N. H. Menzler, A. Hilgers and O. Guillon, *ECS Trans.*, 2023, **111**, 1369.

25 A. Zimmermann, M. Hoffman, B. D. Flinn, R. K. Bordia, T. Chuang, E. R. Fuller and J. Rödel, *J. Am. Ceram. Soc.*, 1998, **81**, 2449–2457.

26 B. D. Flinn, R. K. Bordia, A. Zimmermann and J. Rödel, *J. Eur. Ceram. Soc.*, 2000, **20**, 2561–2568.

27 M. Radovic and E. Lara-Curzio, *Acta Mater.*, 2004, **52**, 5747–5756.

28 N. H. Menzler, J. Malzbender, P. Schoderböck, R. Kauert and H. P. Buchkremer, *Fuel Cells*, 2014, **14**, 96–106.

29 J. Wei, T. Osipova, J. Malzbender and M. Krüger, *Ceram. Int.*, 2018, **44**, 11094–11100.

30 S. Saffirio, S. Anelli, S. Pylypko, M. K. Rath, F. Smeacetto and S. Fiorilli, *Ceram. Int.*, 2024, **50**, 34472–34477.

31 E. Ivers-Tiffée and A. Weber, *J. Ceram. Soc. Jpn.*, 2017, **125**, 193–201.

32 S. Dierickx, A. Weber and E. Ivers-Tiffée, *Electrochim. Acta*, 2020, **355**, 136764.

33 A. Leonide, V. Sonn, A. Weber and E. Ivers-Tiffée, *J. Electrochem. Soc.*, 2007, **155**, B36.

34 C. Endler-Schuck, A. Leonide, A. Weber, S. Uhlenbruck, F. Tietz and E. Ivers-Tiffée, *J. Power Sources*, 2011, **196**, 7257–7262.

35 S. Dierickx, T. Mundloch, A. Weber and E. Ivers-Tiffée, *J. Power Sources*, 2019, **415**, 69–82.

36 R. Chi and Z. Xu, *Metall. Mater. Trans. B*, 1999, **30**, 189–195.

37 Y. Wang, P. Ziemkiewicz and A. Noble, *Minerals*, 2022, **12**, 236.

38 W. Zhang, A. Noble, B. Ji and Q. Li, *J. Rare Earths*, 2022, **40**, 482–490.

39 A. Verma, R. Kore, D. R. Corbin and M. B. Shiflett, *Ind. Eng. Chem. Res.*, 2019, **58**, 15381–15393.

40 Y. M. Park, H. Lim, J.-H. Moon, H.-N. Lee, S. H. Son, H. Kim and H.-J. Kim, *Metals*, 2017, **7**, 303.

41 N. R. Batti and N. R. Mandre, *Metall. Mater. Trans. B*, 2020, **51**, 1225–1232.

42 W. Liu, L. Feng, C. Zhang, H. Yang, J. Guo, X. Liu, X. Zhang and Y. Yang, *J. Mater. Chem. A*, 2013, **1**, 6942–6948.

43 B. Fan, X. Chen, T. Zhou, J. Zhang and B. Xu, *Waste Manage. Res.*, 2016, **34**, 474–481.

44 K. Sahu, R. Sahoo, L. Beshra and M. Mohapatra, *Ionics*, 2021, **27**, 1–14.

45 C. Minu Mary, G. Vimal, P. M. Kamal, J. Gijo, P. R. Biju, J. Cyriac, N. V. Unnikrishnan and M. A. Ittyachen, *J. Mater. Res. Technol.*, 2016, **5**, 268–274.

46 A. B. Yousaf, M. Imran, M. Farooq and P. Kasak, *Sci. Rep.*, 2018, **8**, 4354.

47 B. A. A. Balboul, A. M. El-Roudi, E. Samir and A. G. Othman, *Thermochim. Acta*, 2002, **387**, 109–114.

48 E. D. Bacce, A. M. Pires, M. R. Davalos and M. Jafelicci, *Int. J. Inorg. Mater.*, 2001, **3**, 443–452.

49 P. Venkatesan, Z. H. I. Sun, J. Sietsma and Y. Yang, *Sep. Purif. Technol.*, 2018, **191**, 384–391.

50 F. Liu, C. Peng, B. P. Wilson and M. Lundström, *ACS Sustainable Chem. Eng.*, 2019, **7**, 17372–17378.